Microheater Actuators as a Versatile Platform for Strain Engineering in 2D Materials

Yu Kyoung Ryu, Felix Carrascoso, Rubén López-Nebreda, Nicolás Agraït, Riccardo Frisenda,* and Andres Castellanos-Gomez*

ACCESS | Metrics & More | Article Recommendations | Supporting Information

ABSTRACT: We present microfabricated thermal actuators to engineer the biaxial strain in two-dimensional (2D) materials. These actuators are based on microheater circuits patterned onto the surface of a polymer with a high thermal expansion coefficient. By running current through the microheater one can vary the temperature of the polymer and induce a controlled biaxial expansion of its surface. This controlled biaxial expansion can be transduced to biaxial strain to 2D materials, placed onto the polymer surface, which in turn induces a shift of the optical spectrum. Our thermal strain actuators can reach a maximum biaxial strain of 0.64%, and they can be modulated at frequencies up to 8 Hz. The compact geometry of these actuators results in a negligible spatial drift of 0.03 μm/°C, which facilitates their integration in optical spectroscopy measurements. We illustrate the potential of this strain engineering platform to fabricate a strain-actuated optical modulator with single-layer MoS_2.
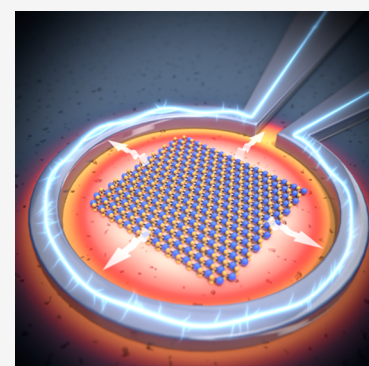
KEYWORDS: strain engineering, 2D materials, MoS_2, microheater, thermal expansion, strain actuator

INTRODUCTION

Two-dimensional (2D) semiconducting materials can withstand exceptionally large mechanical deformations before breakdown (>10% for transition-metal dichalcogenides),[1,2] in contrast to the three-dimensional bulk semiconductors that typically present low failure strains (≤1%) due to the presence of lattice and surface defects.[3−5] This mechanical resilience of 2D semiconductors, due to the absence of dangling bonds in their surface, together with a large strain sensitivity of their band structure make this family of materials of particular interest for strain engineering experiments.[6−13] Interestingly, unlike in strain engineering for bulk semiconductors, which typically relies on applying the strain by forcing the epitaxial growth of materials with dissimilar lattice parameters, for 2D materials there is a rich variety of strategies that allows one to apply a variable strain to them. Moreover, this capability of adjusting the level of strain at will has opened the door to straintronic devices.[14−19]

Here, we demonstrate a platform to achieve fast modulation of biaxial strain in atomically thin MoS_2. Our approach is based on the fabrication of ring-shaped metallic microheaters on top of polypropylene (PP), a polymer substrate with a very large thermal expansion coefficient. The 2D material to be strained is transferred onto the PP surface, in the middle of the ring. Biasing the microheater, we can reliably change the temperature of the PP surface, leading to a controlled biaxial expansion of the PP that is in turn transferred to the MoS_2 flakes.[20,21] We found that these thermal microactuators respond to frequencies up to 8 Hz, which is a factor of

~100 faster compared to that of macroscopic heaters. Moreover, thanks to their compact design and small heating area, our microheaters present a very low spatial thermal drift of ~0.03 μm/°C and are reliable in time, showing good reproducibility in consecutive thermal cycling measurements. We have also estimated the homogeneity of the strain transferred from the microheater to a MoS_2 flake by measuring the spatially resolved differential reflectance across the MoS_2 flake. These measurements reveal very homogeneous strain levels across the whole MoS_2 flake. We finally exploited the control over the strain to demonstrate a fast and large modulation of the refractive index of single-layer MoS_2. All these results point out the superior use of microheaters as a versatile platform to apply and modulate in time biaxial strain in 2D materials in a highly controlled and reversible way.
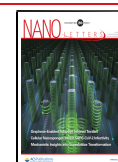
RESULTS AND DISCUSSION

The ring-shaped metallic microheaters are fabricated on PP substrates by optical lithography, metal deposition, and lift-off processes. See the Materials and Methods section for the detailed description of the fabrication steps. PP was chosen as

the substrate because of the combination of its resistance to organic solvents (necessary for the lithographic processing), its high thermal expansion (to yield sizable biaxial strain upon heating), and its high Young's modulus (to ensure a good strain transfer).[20,22] Figure 1a shows optical images of one of the fabricated microheater thermal actuators.
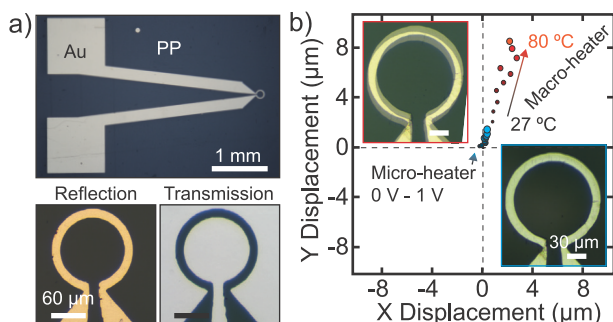

Figure 1. (a) Optical images of the fabricated microheater actuators on a PP substrate with different magnifications. (b) Thermal drift induced by ramping up the temperature with a macroscopic heater (red circles) from 27 to 80 °C and with the microheater (blue circles) from 27 to 75 °C. The top-left inset shows an overlap of two optical images of the sample acquired at 27 and 80 °C using the macroscopic heater. The bottom-right inset shows an overlap of two optical images of the sample acquired at 27 and 75 °C using the microheater.

In the following, we compare the performance of the microheaters with that of macroscopic heaters in terms of thermal drift upon thermal cycling to control biaxial strain in 2D materials. The PP substrate (with the ring-shaped metallic microheater on top) is thermally anchored to a macroscopic Peltier element through thermally conductive tape. Through the text, we denominate 'macroscopic heater configuration' to the use of a Peltier element to increase the global temperature of the whole substrate. Figure 1b shows the in-plane drift in the x and y axis upon temperature increase using either the microheater (blue circles) or the macroscopic heater (red circles) configuration. While the observed drift of the microheater is smaller than ~0.03 μm/°C, the macroscopic heater yields a much sizable drift of ~0.17 μm/°C. The top inset in Figure 1b shows the superposition of optical microscopy images acquired at 27 and 80 °C using the macroscopic heater configuration, where the displacement of the microheater caused by the drift is significant. The bottom inset in Figure 1b shows the superposition of optical microscopy images acquired at V_{heater} = 0 V (27 °C) and V_{heater} = 1 V (corresponding to a temperature of 75 °C in the center of the heater, see SI Section S1 for a complete discussion about the calibration of the temperature in its center upon different biasing conditions) using the microheater configuration. In this latest case, the displacement due to the thermal drift is barely noticeable.

The 2D material that will be subjected to biaxial strain can be placed onto the center of the ring-shaped microheaters right after their fabrication by an all-dry deterministic transfer method.[23−26] The inset in Figure 2a shows an optical image in transmission mode of a single-layer MoS_2 flake transferred in the inner part of the ring microheater. Figure 2a shows differential reflectance spectra measured on the single-layer MoS_2 flake for different bias voltage values applied to the microheater. The differential reflectance spectra display prominent peaks corresponding to the generation of excitons
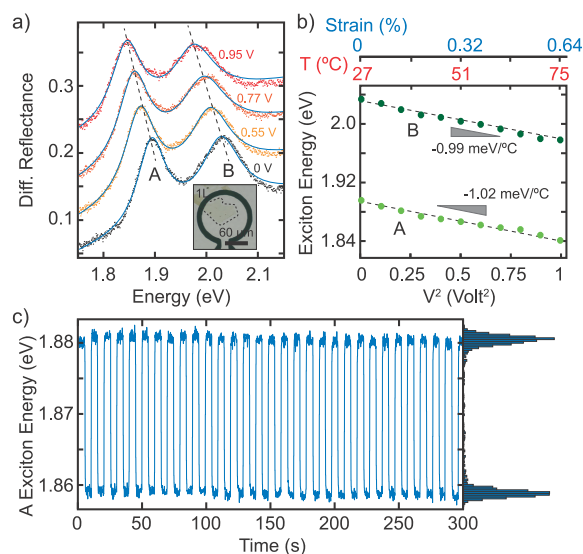

Figure 2. (a) Differential reflectance spectra of a single-layer MoS_2 flake transferred onto the middle of the microheater actuator as a function of the bias voltage applied to the microheater. (Inset) Transmission mode optical image of the device. (b) Energy of the A and B excitons as a function of the square of the voltage applied to the heater (proportional to the electrical power dissipated in the heater). The top axis shows the equivalent substrate temperature and corresponding biaxial biaxial expansion. (c) A exciton energy as a function of time when the microheater is switched between heater-OFF (V_{heater} = 0 V, T = 27 °C) and heater-ON (V_{heater} = 0.52 V, T = 43 °C), corresponding to biaxial strain switched between 0% and 0.21%, using a square signal. The histogram at the right side illustrates the reproducibility of the switching.

in MoS_2.[27,28] We have labeled these features as A and B in accordance with the most extended notation in the literature.[29−31] The red-shift of both A and B excitonic peaks as a function of the applied voltage (-52 meV/V^2, corresponding to -1.02 meV/°C) is a consequence of the temperature increase and the tensile biaxial strain induced on the monolayer by the Joule heating in the microheater.[20,21,32,33] Note that the intrinsic thermal shift of the A and B excitons (without biaxial strain) is -0.4 meV/°C for single-, bi-, and trilayer MoS_2.[21] Therefore, in Figure 2a, a shift of -0.62 meV/°C can be attributed to the biaxial expansion of the MoS_2 lattice.

Figure 2b shows the energy of the excitonic peaks as a function of the square of the voltage applied to the heater (as the substrate temperature, which is linearly proportional to the biaxial expansion, is proportional to the power dissipated by Joule heating V^2/R). One can convert this voltage squared to actual temperature of the PP surface by comparing the spectral shift displayed in Figure 2b (A and B exciton energy vs V^2) with that obtained by turning the microheater OFF and measuring differential reflectance spectra while increasing the temperature using a macroscopic heater equipped with a thermocouple (this measurement yields A and B exciton energy vs temperature of the flake). By dividing the slopes obtained in those two measurements one can get the temperature of the flake as a function of the microheater bias voltage squared (see Section S1 of the Supporting Information for more detailed discussion about the calibration of the flake temperature upon biasing the microheater). The biaxial expansion of the PP substrate (that is transduced to biaxial strain in the flake) can be thus calculated by multiplying
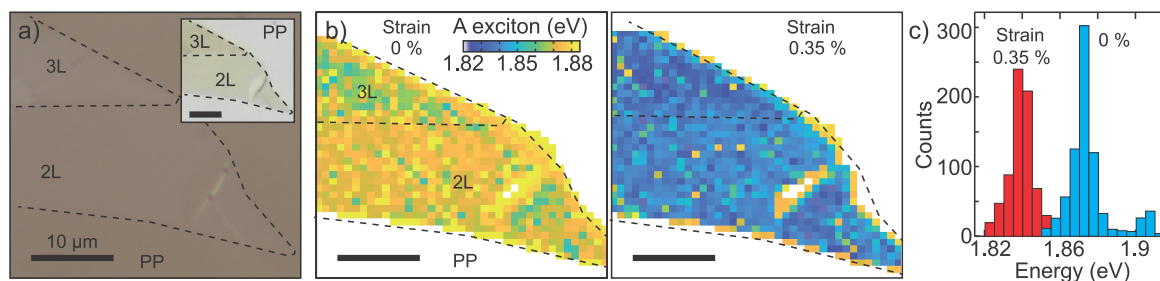
Figure 3. (a) Reflection mode optical image of a bilayer/trilayer MoS₂ flake transferred onto the middle of a microheater actuator. The inset shows the transmission mode optical image of the same flake before transferring it to facilitate the identification of the different regions. (b) Spatial map of the A exciton energy acquired at two different strain levels (0% and 0.35%). (c) Histogram of the A exciton energy values that show very well-defined peaks, illustrating the spatial homogeneity of the induced strain.

the temperature increase (with respect to room temperature) by the PP thermal expansion coefficient of 128×10^{-6} °C^{-1}, determined in previous works.[20,21] Then, we determine the gauge factor of the A and B excitons, that is, the spectral shift per percent of biaxial strain, from the slope of the linear fits of the graphs in Figure 2b, after subtracting the intrinsic thermal shift value mentioned above, being 48 meV/% and 46 meV/%, respectively. Figure S2 shows additional measurements performed on a bilayer MoS₂ that shows a strain gauge factor of 55, 50, and 60 meV/% for the A, B, and IL (interlayer) excitons, respectively. Figure S3 shows other measurements on a trilayer MoS₂ with a strain gauge factor of 32 and 25 meV/% for the A and B excitons, respectively. These values are compatible with those obtained with macroscopic heaters.[20,21] The maximum strain level that can be applied with the microheaters actuators is +0.64% and it is limited by the melting temperature of the PP substrate as at higher microheater biasing conditions the PP substrate close to the metal electrodes starts to melt down.

The reproducibility of the spectral shift induced by the microheater was tested on a trilayer MoS₂ flake by applying 30 cycles of heater-OFF (V_{heater} = 0 V) and heater-ON (V_{heater} = 0.52 V) states, which correspond to 0% and 0.21% of biaxial strain, respectively (Figure 2c). The A exciton energy reproducibly switches between two well-defined values (~1.88 and ~1.86 eV) when the strain is switched between 0% and 0.21%, respectively. At the right side of Figure 2c we show a histogram to quantify the reproducibility. Optical images of the device in reflection and transmission optical microscopy modes and the differential reflectance spectra at the two levels of strain can be found in Figure S3.

The uniformity of the induced biaxial strain by the microheater actuator has been checked by spatially mapping the differential reflectance on a bilayer/trilayer MoS₂ flake transferred in the center of a microheater. Figure 3a shows the optical image of the flake on the PP surface acquired in reflection mode. A first mapping of the flake, with an area of around 320 μm^2, was performed at 0% strain (room temperature), see the left panel in Figure 3b. The same area was then mapped under a strain of 0.35% (right panel in Figure 3b). The spatial variation of the energy of the A exciton is shown in the colormaps displayed in Figure 3b. Both panels of Figure 3b and the histogram extracted from the maps, shown in Figure 3c, prove the highly uniform strain applied by the thermal actuation of the ring-shaped microheaters. Therefore, although one expects a higher temperature at the close vicinity of the metal electrodes, the temperature in the central part of the microheater does not have a sizable spatial variation.

Next, we compare the operation speed of the microheater with respect to the macroscopic heater configuration. To do so, we have used the same trilayer MoS₂ tested in Figure 2c. We have monitored the position of the A exciton as a function of time while we turn ON and OFF the heaters (Figure 4a).
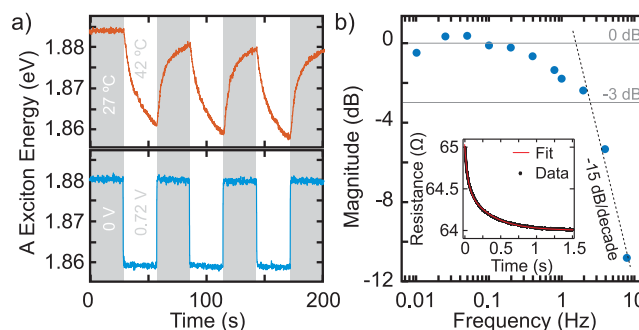

Figure 4. (a) A exciton energy as a function of time while the heater is switched ON and OFF. In the top panel the results of using a macroscopic heater are shown, and in the bottom panel we show the same experiment switching ON and OFF a microheater thermal actuator. (b) Frequency response of the microheater actuator. The inset shows the normalized resistance change of a microheater when the bias voltage is suddenly reduced from 0.5 to 0.3 V. The data have been fitted to an exponential decay function (red curve).

The direct comparison shows that the microheater response is almost instantaneous, being of the same order as the spectra acquisition time of our spectrometer (110 ms), while the macroscopic heater one is around 2 orders of magnitude slower. This result is another fundamental advantage of microheaters compared to macroheaters to control the biaxial strain in 2D materials. The response of the microheaters as a function of the frequency was also directly measured by monitoring the modulation amplitude of the A exciton energy while the microheater is biased with a sinusoidal wave of increasing frequency (Figure 4b), obtaining a cutoff frequency of 2.5 Hz and a sizable response even up to 8 Hz. Similarly, the time-resolved response in the resistance of the microheater to a step change in the biasing voltage (from 0.5 to 0.3 V) shows an exponential decay with a time constant of 0.35 s, which corresponds to a frequency of 2.8 Hz that is comparable to the cutoff frequency estimated from the frequency response (inset from Figure 4b).

The capability of fast modulating the strain on 2D materials in a reliable way opens possibilities to use these microheater thermal actuators in optical modulation applications.[34−37] Figure 5a shows the time evolution of the differential
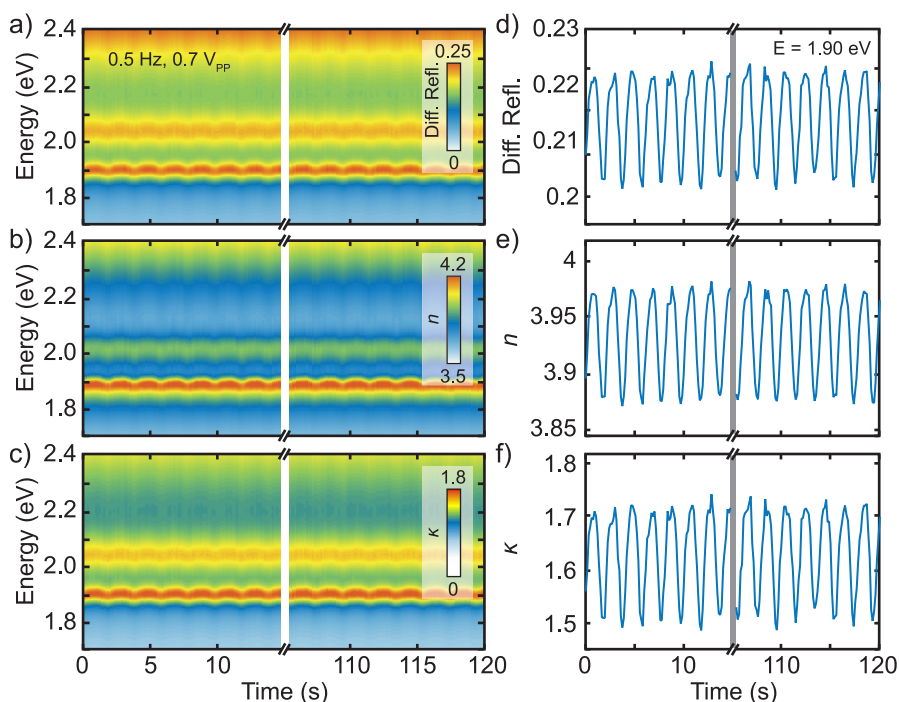
Figure 5. (a) Colormap of the differential reflectance of a single-layer MoS$_2$ flake applying a sine wave modulated voltage to the microheater (frequency = 0.5 Hz, amplitude = 0.7 V$_{pp}$, sampling rate = 10 Hz). (b, c) Colormaps of the real part n (b) and imaginary part κ (c) of the complex refractive index of single-layer MoS$_2$ calculated from the differential reflectance map of panel (a). (d−f) Horizontal linecuts extracted from the maps of panels (a−c) at an energy of 1.9 eV.

reflectance spectra of a single-layer MoS$_2$ flake when the microheater is biased with an AC voltage (0.7 V$_{pp}$ and 0.5 Hz). As expected from the previous measurements, the excitonic features present in the differential reflectance spectra are shifted following the AC driving signal fed into the microheater, and this modulation is quite reliable over more than 60 cycles. Interestingly, using the Fresnel equations for the three optical media (air/MoS$_2$/PP) combined with a Kramers−Kronig analysis, we can extract the two components of the complex refractive index from the measured differential reflectance spectra. Figure 5b and 5c show the time evolution of the real- (n) and imaginary-part (κ) of the complex index of refraction of 1L-MoS$_2$. Both these quantities accurately follow the strain modulation imposed by the microheater thermal actuator. In order to better quantify the magnitude of the strain-induced optical modulation in the single-layer MoS$_2$, Figures 5d, 5e, and 5f display linecuts of Figure 5a, 5b, and 5c, respectively, at an energy of 1.9 eV (653 nm of wavelength). According to Figure 5d, the AC strain modulation introduces a remarkable variation in the differential reflectance amplitude of 11%, at the probed energy of 1.9 eV. The modulation of n and κ also reach 2.5% and 13%, respectively, which is significantly larger than the refractive index modulation achieved with thermally actuated dielectric-based optical modulators (1.1%).[37] This motivates the potential use of these microheater thermal strain actuators to fabricate 2D-based optical modulators. The main limitation of these thermal strain actuators, however, is to reach very high operation speed. A simple way to increase the operation speed is to reduce the thickness of the substrate. Indeed, the response time of the heater can be expected to be $\sim t^2/\alpha$, where t is the thickness and α is the thermal diffusivity of the PP. A further improvement in the operation speed by a factor of 100−

1000 can be achieved by reducing the dimensions of the microheaters. In fact, Quidant and co-workers recently demonstrated that microheaters 10 μm in diameter can operate at frequencies up to ∼3.5 kHz.[37]

■ CONCLUSION

In summary, we introduce the use of thermal actuators based on microheaters fabricated on PP substrate for strain engineering in 2D materials. We demonstrate that these actuators are a versatile and straightforward platform to control the biaxial strain in atomically thin MoS$_2$ layers. We show how these thermal actuators allow us to apply a maximum strain of 0.64% that can be reliably modulated at 8 Hz with a negligible spatial drift of 0.03 μm/°C. We also demonstrate a strain-actuated optical modulator, based on single-layer MoS$_2$ and our microheater strain actuator, showing a large modulation of the refractive index. In conclusion, we introduced a straining platform to apply biaxial strain to 2D materials and nanomaterials in general.

■ MATERIALS AND METHODS

Microheaters Fabrication. PP substrates of 200 μm thickness (Fellowes, U.S.) have been flattened to ensure their uniformity prior to the lithographic processing. To accomplish this, we fix the PP substrate to a SiO$_2$/Si substrate with kapton tape. Then, we spin-coat TI 35ESX resist (MicroChemicals, Germany) at 3000 rpm for 30 s on the substrate. The substrate is soft baked at 100 °C for 3 min on a hot plate. Then, the substrate is exposed by blue light (430−470 nm) for 2.5−3 s with a 2.5× objective using a Smart Print (Microlight3D, France) maskless photolithography system. After developing the substrates in a solution consisting in 2 parts AZ Developer (MicroChemicals, Germany) to 1 part DI H$_2$O for 50 s, the

exposed parts of the resist are removed. Finally, a 5 nm Ti/50 nm Au thick layer is deposited on the substrates by electron-beam evaporation. Finally, the residual photoresist is stripped by a lift-off process via immersing the samples on a TechniStrip Micro D350 (dimethyl sulfoxide, MicroChemicals, Germany) solution at 60 °C. For some samples, a gentle sonication for 30−60 s can be applied if required.

Transfer of the MoS$_2$ Few Layers to the Microheaters. The MoS$_2$ few-layers were mechanically exfoliated from a natural molybdenite mineral crystal (Molly Hill mine, Quebec, Canada) with Nitto tape (Nitto SPV 224) and then transferred onto Gel-film (Gel-Pak, WF 4× 6.0 mil), which is a commercially available polydimethylsiloxane (PDMS) sub-strate. Prior to the transfer, the thickness of the flakes was determined by quantitative analysis of transmission mode optical images and by micro-differential reflectance spectros-copy.[38,39] After thickness characterization, the chosen flakes were transferred onto the center of the ring-shaped micro-heaters contained on the PP substrates by a dry deterministic transfer method.[23−25]

Differential Reflectance Measurements. The optical microscopy images and differential reflection spectroscopy measurements were acquired with a Motic BA MET310-T microscope with a fiber-coupled CCD spectrometer (Thorlabs CCS200/M). The details of the equipment setup are explained elsewhere.[27]

Spatial Mapping of the Differential Reflectance. To perform the spatial mapping of the differential reflectance, we used a setup similar to the one described above consisting of a Motic BA310Met-H microscope operated in epi-illumination mode with a fiber-coupled CCD spectrometer (Thorlabs CCS200/M, external trigger mode) attached to a TENMA programmable benchtop power supply to supply the trigger voltage. The sample was mounted below the microscope objective onto an $x-y$ motorized translation stage (EKSMA optics 2× 960-0070-03LS motorized translation stage and 980-0942 2-axis translational stage controller). We control the TENMA voltage source and the $x-y$ motorized stage through a homemade routine written in Matlab, which performs a raster scan in the x and y directions with a user defined step-size and at every point stops to acquire a reflectance spectrum.

Microheater Configuration. The voltage is applied by a TENMA programmable benchtop power supply, and the current vs voltage ($I-V$) curves as a function of the temperature are measured with a source-measure unit (Keithley 2450).

Time-resolved Resistance Measurement on Micro-heater. The time response of the microheater was obtained by measuring the resistance in a 4-terminal configuration using a Zurich Instruments HF2LI lock-in amplifier and an AC voltage at high frequency (∼20 kHz) to bias the microheater.

Macro-heater Configuration. The PP substrate contain-ing the microheater plus MoS$_2$ flake are thermally anchored onto a Peltier (TEC1-12706) with thermally conductive tape. This allows us to regulate the temperature of the whole substrate−heater−flake system with the macroscopic heater. The temperature is measured by a thermocouple attached to the Peltier surface in proximity of the sample. We have checked that attaching the thermocouple on the surface of the PP substrate leads to a temperature difference of ∼1 °C with respect to temperature on the Peltier surface.

■ ASSOCIATED CONTENT

Ⓢ Supporting Information

The Supporting Information is available free of charge at https://pubs.acs.org/doi/10.1021/acs.nanolett.0c01706.

Calibration of the microheater's power-to-temperature conversion, additional measurements of biaxial strain in MoS$_2$ flakes, and strain-amplified thermoreflectance spectroscopy (PDF)

■ AUTHOR INFORMATION

Corresponding Authors

Riccardo Frisenda − *Materials Science Factory, Instituto de Ciencia de Materiales de Madrid (ICMM-CSIC), E-28049 Madrid, Spain;* ⓞ orcid.org/0000-0003-1728-7354; Email: riccardo.frisenda@csic.es

Andres Castellanos-Gomez − *Materials Science Factory, Instituto de Ciencia de Materiales de Madrid (ICMM-CSIC), E-28049 Madrid, Spain;* ⓞ orcid.org/0000-0002-3384-3405; Email: andres.castellanos@csic.es

Authors

Yu Kyoung Ryu − *Materials Science Factory, Instituto de Ciencia de Materiales de Madrid (ICMM-CSIC), E-28049 Madrid, Spain;* ⓞ orcid.org/0000-0002-5000-2974

Felix Carrascoso − *Materials Science Factory, Instituto de Ciencia de Materiales de Madrid (ICMM-CSIC), E-28049 Madrid, Spain*

Rubén López-Nebreda − *Departamento de Física de la Materia Condensada, Universidad Autónoma de Madrid, E-28049 Madrid, Spain*

Nicolás Agraït − *Departamento de Física de la Materia Condensada and Condensed Matter Physics Center (IFIMAC) and Instituto "Nicolás Cabrera", Universidad Autónoma de Madrid, E-28049 Madrid, Spain; Fundación IMDEA Nanociencia, Ciudad Universitaria de Cantoblanco, E-28049 Madrid, Spain;* ⓞ orcid.org/0000-0003-4840-5851

Complete contact information is available at:
https://pubs.acs.org/10.1021/acs.nanolett.0c01706

Notes

The authors declare no competing financial interest.

■ REFERENCES

(1) Bertolazzi, S.; Brivio, J.; Kis, A. Stretching and Breaking of Ultrathin MoS2. *ACS Nano* **2011**, *5* (12), 9703−9709.

(2) Cooper, R. C.; Lee, C.; Marianetti, C. A.; Wei, X.; Hone, J.; Kysar, J. W. Nonlinear Elastic Behavior of Two-Dimensional Molybdenum Disulfide. *Phys. Rev. B: Condens. Matter Mater. Phys.* **2013**, *87* (3), 035423.

(3) Castellanos-Gomez, A.; Singh, V.; van der Zant, H. S. J. H. S. J.; Steele, G. A. G. A. Mechanics of Freely-Suspended Ultrathin Layered Materials. *Ann. Phys.* **2015**, *527* (1−2), 27−44.

(4) Akinwande, D.; Brennan, C. J.; Bunch, J. S.; Egberts, P.; Felts, J. R.; Gao, H.; Huang, R.; Kim, J. S.; Li, T.; Li, Y.; Liechti, K. M.; Lu, N.; Park, H. S.; Reed, E. J.; Wang, P.; Yakobson, B. I.; Zhang, T.; Zhang, Y. W.; Zhou, Y.; Zhu, Y. A Review on Mechanics and Mechanical Properties of 2D Materials—Graphene and Beyond. *Extrem. Mech. Lett.* **2017**, *13*, 42−77.

(5) Deng, S.; Sumant, A. V.; Berry, V. Strain Engineering in Two-Dimensional Nanomaterials beyond Graphene. *Nano Today* **2018**, *22*, 14−35.

(6) Roldán, R.; Castellanos-Gomez, A.; Cappelluti, E.; Guinea, F. Strain Engineering in Semiconducting Two-Dimensional Crystals. *J. Phys.: Condens. Matter* **2015**, *27* (31), 313201.

(7) Amorim, B.; Cortijo, A.; de Juan, F.; Grushin, A. G.; Guinea, F.; Gutiérrez-Rubio, A.; Ochoa, H.; Parente, V.; Roldán, R.; San-Jose, P.; Schiefele, J.; Sturla, M.; Vozmediano, M. A. H. Novel Effects of Strains in Graphene and Other Two Dimensional Materials. *Phys. Rep.* **2016**, *617*, 1−54.

(8) Conley, H. J.; Wang, B.; Ziegler, J. I.; Haglund, R. F.; Pantelides, S. T.; Bolotin, K. I. Bandgap Engineering of Strained Monolayer and Bilayer MoS$_2$. *Nano Lett.* **2013**, *13* (8), 3626−3630.

(9) He, K.; Poole, C.; Mak, K. F.; Shan, J. Experimental Demonstration of Continuous Electronic Structure Tuning via Strain in Atomically Thin MoS2. *Nano Lett.* **2013**, *13* (6), 2931−2936.

(10) Castellanos-Gomez, A.; Roldán, R.; Cappelluti, E.; Buscema, M.; Guinea, F.; van der Zant, H. S. J.; Steele, G. A. Local Strain Engineering in Atomically Thin MoS2. *Nano Lett.* **2013**, *13* (11), 5361−5366.

(11) Hui, Y. Y.; Liu, X.; Jie, W.; Chan, N. Y.; Hao, J.; Hsu, Y.-T.; Li, L.-J.; Guo, W.; Lau, S. P. Exceptional Tunability of Band Energy in a Compressively Strained Trilayer MoS2 Sheet. *ACS Nano* **2013**, *7* (8), 7126−7131.

(12) Dai, Z.; Liu, L.; Zhang, Z. Strain Engineering of 2D Materials: Issues and Opportunities at the Interface. *Adv. Mater.* **2019**, *31* (45), 1805417.

(13) Lloyd, D.; Liu, X.; Christopher, J. W.; Cantley, L.; Wadehra, A.; Kim, B. L.; Goldberg, B. B.; Swan, A. K.; Bunch, J. S. Band Gap Engineering with Ultralarge Biaxial Strains in Suspended Monolayer MoS 2. *Nano Lett.* **2016**, *16* (9), 5836−5841.

(14) Manzeli, S.; Allain, A.; Ghadimi, A.; Kis, A. Piezoresistivity and Strain-Induced Band Gap Tuning in Atomically Thin MoS $_2$. *Nano Lett.* **2015**, *15* (8), 5330−5335.

(15) Quereda, J.; Palacios, J. J.; Agräit, N.; Castellanos-Gomez, A.; Rubio-Bollinger, G. Strain Engineering of Schottky Barriers in Single- and Few-Layer MoS2 Vertical Devices. *2D Mater.* **2017**, *4* (2), 021006.

(16) Gant, P.; Huang, P.; Pérez de Lara, D.; Guo, D.; Frisenda, R.; Castellanos-Gomez, A. A Strain Tunable Single-Layer MoS2 Photo-detector. *Mater. Today* **2019**, *27*, 8−13.

(17) Wang, L.; Zihlmann, S.; Baumgartner, A.; Overbeck, J.; Watanabe, K.; Taniguchi, T.; Makk, P.; Schönenberger, C. In Situ Strain Tuning in HBN-Encapsulated Graphene Electronic Devices. *Nano Lett.* **2019**, *19* (6), 4097−4102.

(18) Tong, L.; Duan, X.; Song, L.; Liu, T.; Ye, L.; Huang, X.; Wang, P.; Sun, Y.; He, X.; Zhang, L.; et al. Artificial Control of In-Plane Anisotropic Photoelectricity in Monolayer MoS2. *Appl. Mater. Today* **2019**, *15*, 203−211.

(19) Iff, O.; Tedeschi, D.; Martín-Sánchez, J.; Moczała-Dusanowska, M.; Tongay, S.; Yumigeta, K.; Taboada-Gutiérrez, J.; Savaresi, M.; Rastelli, A.; Alonso-González, P.; et al. Strain-Tunable Single Photon Sources in WSe2Monolayers. *Nano Lett.* **2019**, *19* (10), 6931−6936.

(20) Frisenda, R.; Drüppel, M.; Schmidt, R.; Michaelis de Vasconcellos, S.; Perez de Lara, D.; Bratschitsch, R.; Rohlfing, M.;

Castellanos-Gomez, A. Biaxial Strain Tuning of the Optical Properties of Single-Layer Transition Metal Dichalcogenides. *npj 2D Mater. Appl.* **2017**, *1* (1), 10.

(21) Carrascoso, F.; Lin, D.-Y.; Frisenda, R.; Castellanos-Gomez, A. Biaxial Strain Tuning of Interlayer Excitons in Bilayer MoS 2. *J. Phys. Mater.* **2020**, *3* (1), 015003.

(22) Frisenda, R.; Schmidt, R.; Michaelis De Vasconcellos, S.; Bratschitsch, R.; Perez De Lara, D.; Castellanos-Gomez, A. Biaxial Strain in Atomically Thin Transition Metal Dichalcogenides. *Proceedings of SPIE - The International Society for Optical Engineering* **2017**, *10353*, 22.

(23) Castellanos-Gomez, A.; Buscema, M.; Molenaar, R.; Singh, V.; Janssen, L.; van der Zant, H. S. J. H. S. J.; Steele, G. A. G. A. Deterministic Transfer of Two-Dimensional Materials by All-Dry Viscoelastic Stamping. *2D Mater.* **2014**, *1* (1), 011002.

(24) Frisenda, R.; Navarro-Moratalla, E.; Gant, P.; Pérez De Lara, D.; Jarillo-Herrero, P.; Gorbachev, R. V.; Castellanos-Gomez, A. Recent Progress in the Assembly of Nanodevices and van Der Waals Heterostructures by Deterministic Placement of 2D Materials. *Chem. Soc. Rev.* **2018**, *47* (1), 53−68.

(25) Gant, P.; Carrascoso, F.; Zhao, Q.; Ryu, Y. K.; Seitz, M.; Prins, F.; Frisenda, R.; Castellanos-Gomez, A. A System for the Deterministic Transfer of 2D Materials under Inert Environmental Conditions. *2D Mater.* **2020**, *7* (2), 025034.

(26) Zhao, Q.; Wang, T.; Ryu, Y. K.; Frisenda, R.; Castellanos-Gomez, A. An Inexpensive System for the Deterministic Transfer of 2D Materials. *J. Phys. Mater.* **2020**, *3* (1), 016001.

(27) Frisenda, R.; Niu, Y.; Gant, P.; Molina-Mendoza, A. J.; Schmidt, R.; Bratschitsch, R.; Liu, J.; Fu, L.; Dumcenco, D.; Kis, A.; De Lara, D. P.; Castellanos-Gomez, A. Micro-Reflectance and Transmittance Spectroscopy: A Versatile and Powerful Tool to Characterize 2D Materials. *J. Phys. D: Appl. Phys.* **2017**, *50* (7), 074002.

(28) Niu, Y.; Gonzalez-Abad, S.; Frisenda, R.; Marauhn, P.; Drüppel, M.; Gant, P.; Schmidt, R.; Taghavi, N. S.; Barcons, D.; Molina-Mendoza, A. J.; de Vasconcellos, S. M.; Bratschitsch, R.; Perez De Lara, D.; Rohlfing, M.; Castellanos-Gomez, A. Thickness-Dependent Differential Reflectance Spectra of Monolayer and Few-Layer MoS2, MoSe2, WS2 and WSe2. *Nanomaterials* **2018**, *8* (9), 725.

(29) Qiu, D. Y.; da Jornada, F. H.; Louie, S. G. Optical Spectrum of MoS2: Many-Body Effects and Diversity of Exciton States. *Phys. Rev. Lett.* **2013**, *111* (21), 216805.

(30) Schmidt, R.; Niehues, I.; Schneider, R.; Drüppel, M.; Deilmann, T.; Rohlfing, M.; De Vasconcellos, S. M. S. M.; Castellanos-Gomez, A.; Bratschitsch, R. Reversible Uniaxial Strain Tuning in Atomically Thin WSe2. *2D Mater.* **2016**, *3* (2), 021011.

(31) Niehues, I.; Blob, A.; Stiehm, T.; Michaelis de Vasconcellos, S.; Bratschitsch, R. Interlayer Excitons in Bilayer MoS 2 under Uniaxial Tensile Strain. *Nanoscale* **2019**, *11*, 12788−12792.

(32) Plechinger, G.; Castellanos-Gomez, A.; Buscema, M.; van der Zant, H. S. J.; Steele, G. A.; Kuc, A.; Heine, T.; Schüller, C.; Korn, T. Control of Biaxial Strain in Single-Layer Molybdenite Using Local Thermal Expansion of the Substrate. *2D Mater.* **2015**, *2* (1), 015006.

(33) Huang, S.; Zhang, G.; Fan, F.; Song, C.; Wang, F.; Xing, Q.; Wang, C.; Wu, H.; Yan, H. Strain-Tunable van Der Waals Interactions in Few-Layer Black Phosphorus. *Nat. Commun.* **2019**, *10* (1), 2447.

(34) Yu, Y.; Yu, Y.; Huang, L.; Peng, H.; Xiong, L.; Cao, L. Giant Gating Tunability of Optical Refractive Index in Transition Metal Dichalcogenide Monolayers. *Nano Lett.* **2017**, *17* (6), 3613−3618.

(35) Vella, D.; Ovchinnikov, D.; Martino, N.; Vega-Mayoral, V.; Dumcenco, D.; Kung, Y. C.; Antognazza, M. R.; Kis, A.; Lanzani, G.; Mihailovic, D.; Gadermaier, C. Unconventional Electroabsorption in Monolayer MoS2. *2D Mater.* **2017**, *4* (2), 021005.

(36) Newaz, A. K. M.; Prasai, D.; Ziegler, J. I.; Caudel, D.; Robinson, S.; Haglund, R. F., Jr; Bolotin, K. I. Electrical Control of Optical Properties of Monolayer MoS2. *Solid State Commun.* **2013**, *155*, 49−52.

(37) Berto, P.; Philippet, L.; Osmond, J.; Liu, C. F.; Afridi, A.; Montagut Marques, M.; Molero Agudo, B.; Tessier, G.; Quidant, R.

Tunable and Free-Form Planar Optics. *Nat. Photonics* **2019**, *13* (9), 649−656.

(38) Niu, Y.; Gonzalez-Abad, S.; Frisenda, R.; Marauhn, P.; Drüppel, M.; Gant, P.; Schmidt, R.; Taghavi, N.; Barcons, D.; Molina-Mendoza, A.; de Vasconcellos, S.; Bratschitsch, R.; Perez De Lara, D.; Rohlfing, M.; Castellanos-Gomez, A. Thickness-Dependent Differential Reflectance Spectra of Monolayer and Few-Layer MoS2, MoSe2, WS2 and WSe2. *Nanomaterials* **2018**, *8* (9), 725.

(39) Taghavi, N. S.; Gant, P.; Huang, P.; Niehues, I.; Schmidt, R.; Michaelis de Vasconcellos, S.; Bratschitsch, R.; García-Hernández, M.; Frisenda, R.; Castellanos-Gomez, A. Thickness Determination of MoS2, MoSe2, WS2 and WSe2 on Transparent Stamps Used for Deterministic Transfer of 2D Materials. *Nano Res.* **2019**, *12* (7), 1691−1695.